DNA Binding of an Organic dppz-Based Intercalator†

Tim Phillips, Ihtshamul Haq, Anthony J. H. M. Meijer, Harry Adams, Ian Soutar, Linda Swanson, Matthew J. Sykes, and Jim A. Thomas*

Department of Chemistry, University of Sheffield, Sheffield S3 7HF, U.K.

Received April 28, 2004; Revised Manuscript Received August 20, 2004

ABSTRACT: An improved synthesis of a water-soluble derivative of dipyrido[3,2-*a*:2′,3′-*c*]phenazine (dppz) is reported. The structures of both dppz and the cation ethylene-bipyridyldiylium-phenazine dinitrate {[**1**][$(PF_6)_2$]} have been obtained via X-ray crystallography. Metal complex derivatives of dppz are very well studied. However, using the water soluble [**1**][$(NO_3)_2$], the nature of the interaction of a simple dppz unit with duplex DNA has been investigated for the first time. In both organic solvents and water, **1** displays unstructured luminescence, assigned to an intramolecular charge transfer. The emission is quenched on binding to natural and synthetic duplex DNA, including poly(dA)·poly(dT). A variety of techniques reveal that the cation binds to DNA with an affinity comparable to those of many metal dppz complexes, via an intercalative binding mode.

The interactions of small molecules with DNA have attracted a great deal of attention (*1*). The two most common noncovalent binding motifs for such systems are groove binding (*2*−*4*) or intercalation (*5*, *6*). Many therapeutic agents, particularly anticancer drugs, are known to bind DNA via these motifs, and the possibility of gene modulation by sequence specific binding of small molecules to DNA has also been pursued (*7*, *8*). In related work, metal complexes have been used to probe the structural and physical properties of DNA (*9*−*13*).

In this latter context, complexes containing the organic ligand dipyrido[3,2-*a*:2′,3′-*c*]phenazine (dppz)[1] have been much studied, particularly the Ru^{II} complexes, $[Ru(bpy)_2(dppz)]^{2+}$ and $[Ru(phen)_2(dppz)]^{2+}$ (bpy = 2,2′-bipyridine, phen = 1,10-phenanthroline) (*14*) (Scheme 1).

These complexes exhibit distinctive photophysical properties: measurements have shown that in both the ground and excited states the charge transfer is directed from the metal center to the phenazine of the dppz ligand. The major nonradiative deactivation pathway of the excited state is via hydrogen bonding to the phenazine nitrogen atoms (*15*, *16*). This leads to the excited state being very dependent on its microenvironment: while emission from a triplet $Ru^{II} \rightarrow$ dppz metal-to-ligand charge transfer (MLCT) manifold is quenched in protic solvents, addition of DNA enhances the luminescence by several orders of magnitude. Although the precise details of the interaction with DNA are still a matter of some debate (*17*−*21*), it is known that this "light-switch" effect is due to intercalation of the dppz unit into the DNA duplex (*22*). This interaction results in high DNA binding affinities: $K_b \geq 10^6\ M^{-1}$. Consequent studies on a variety of different metal centers have resulted in related dppz complexes (*23*−*29*).

Scheme 1: Structures Relevant to This Report

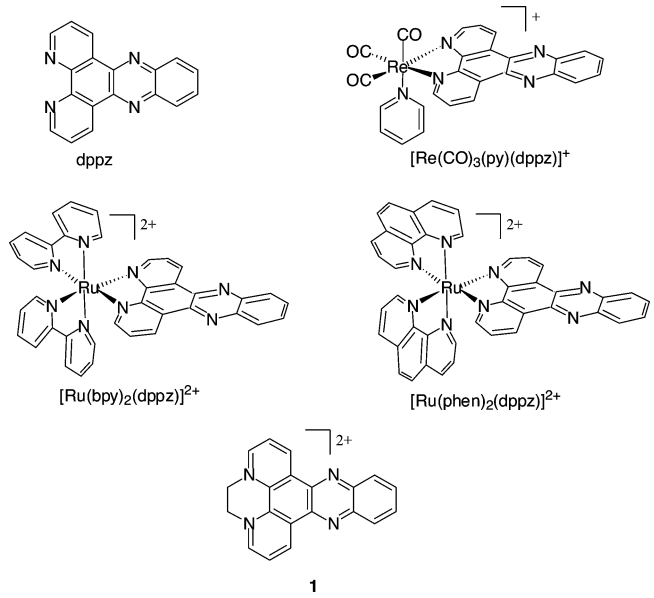

Despite the large amount of interest in coordination complexes of dppz, the DNA binding properties of organic derivatives of this moiety have yet to be investigated. As a planar aromatic molecule, dppz itself is virtually insoluble in aqueous solutions. However, the previously reported dicationic bromide salt of the dppz derivative (**1**, Scheme 1) is known to show good water solubility and is stable at neutral pH. Apart from the report of its synthesis and a brief investigation of its redox behavior (*30*), **1** has not been investigated. Herein, we report an initial exploration of the photophysical and DNA binding properties of this "bare" dppz intercalative moiety.

† We gratefully acknowledge the support of The Royal Society (J.A.T.) and EPSRC (I.H.).

* To whom correspondence should be addressed. Fax: +(114) 273-8673. Phone: +(114) 222-9325. E-mail: james.thomas@sheffield.ac.uk.

[1] Abbreviations: **1**, ethylene-bipyridyldiylium-phenazine dinitrate; bpy, 2,2′-bipyridine; DFT, density functional theory; dppz, dipyrido-[3,2-*a*:2′,3′-*c*]phenazine; ICT, intramolecular charge transfer; ITC, isothermal calorimetry; MLCT, metal-to-ligand charge transfer; phen, 1,10-phenanthroline.

10.1021/bi049146r CCC: $27.50
Published on Web 10/09/2004

MATERIALS AND METHODS

Materials. Commercially available materials were used as received. All reactions were carried out under an inert argon atmosphere. dppz was synthesized via a literature procedure (*30*). Calf thymus DNA (CT-DNA) was purchased from Sigma and was purified until $A_{260}/A_{280} > 1.9$. Concentrations of DNA solutions were determined spectroscopically using the extinction coefficient of CT-DNA ($\epsilon = 6600$ mol^{-1} dm^3 cm^{-1}) at 260 nm. The buffer used for titrations consisted of 25 mM NaCl and 5 mM Tris (pH 7.0) made with doubly distilled water (Millipore).

Instrumentation. Electronic spectra were recorded on a Carey Bio-3 UV−visible spectrophotometer. Emission spectra were recorded on a Hitachi fluorimeter. NMR spectra (400 MHz) were recorded on a Bruker instrument with offline data analysis performed on an IBM personal computer running Bruker win-NMR software. FAB mass spectra were obtained on a Kratos MS80 machine working in the positive ion mode, with a *m*-nitrobenzyl alcohol matrix. ITC experiments were conducted using a VP-ITC (*31*, *32*) from MicroCal LLC (Northampton, MA) interfaced with a Gateway PIII personal computer. Data acquisition and analysis were performed using Origin 5.0 (MicroCal LLC), and all titrations were performed at 25 °C in the 5 mM Tris, 25 mM NaCl, pH 7.0 buffer.

The time-resolved anisotropy experiments were carried out on an Edinburgh Instruments 199 time-correlated single-photon counter spectrometer. It was set to accumulate fluorescence data in planes parallel and perpendicular to the excitation wavelength. The excitation source was a nanoLED05 nanosecond diode with a maximum excitation wavelength of 450 nm. A 500 nm interference filter was also used that transmits waves of 500 ± 10 nm. A 2.5×10^{-4} M solution of [**1**][$(NO_3)_2$] added to a 3 mL cuvette of 5 mM Tris and 25 mM NaCl was run first. Then DNA was added to this cuvette, to result in an approximately 50% bound situation.

*Synthesis of [**1**][$(PF_6)_2$]*. An improved synthesis adapted from the original method of Dickson and Summers (*21*) was employed. dppz (0.8167 g, 2.89 mM) and 1,2-dibromoethane (50 mL) were brought to gentle reflux. The solution changed from orange to red, and after 20 min, a yellow precipitate of the product began to form. After 2 h, the solution was cooled to room temperature and the yellow precipitate was collected by filtration and washed with cold ethanol. The solid that remained was dissolved into a small amount of water (5 mL) and then filtered. Excess ammonium hexafluorophosphate was added to the filtrate, resulting in the precipitation of [**2**][$(PF_6)_2$] as an off-white microcrystalline powder, which was filtered and dried overnight *in vacuo*: 0.6191 g (69%) yield; ^{1}H NMR (acetone-d_6) δ 6.12 (t, 4H), 8.30 (dd, 2H), 8.63 (dd, 2H), 9.12 (dd, 2H), 10.01 (dd, 2H), 10.69 (dd, 2H); FAB-MS *m*/*z* (%) 309 (100) [$M^+ - 2(PF_6)$], 283 (75) [$M^+ - 2(PF_6) -$ Et], 155 (15) [$M^{2+} - 2(PF_6)$]. Anal. Found: C, 39.73; H, 2.31; N, 9.06. Calcd for $C_{20}H_{14}N_4P_2F_{12}$: C, 40.02; H, 2.35; N, 9.33.

X-ray Crystallography. X-ray quality crystals of dppz were obtained by slow cooling from a saturated DMSO solution of a sample of dppz that had previously been recrystallized from methanol and water. Crystals of [**2**][$(PF_6)_2$] were obtained from the vapor diffusion of diethyl ether into a nitromethane solution. In both cases, data that were collected were recorded on a Bruker Smart CCD area detector with an Oxford Cryosystems low-temperature system. Cell parameters were refined from the setting angles of 2021 reflections (θ range of 1.63−28.33°) for dppz and 3833 reflections (θ range of 0.91−23.27°) for [**1**][$(PF_6)_2$]. Reflections were measured from a hemisphere of data collected of frames each covering 0.3° in ω. All reflections were corrected for Lorentz and polarization effects and for absorption by semiempirical methods based on symmetry-equivalent and repeated reflections. The structure was determined by direct methods and refined by full matrix least-squares methods on F^2. Hydrogen atoms were placed geometrically and refined with a riding model (including torsional freedom for methyl groups), and with U_{iso} constrained to 1.2 (1.5 for methyl groups) times the U_{eq} of the carrier atom. Complex scattering factors were taken from SHELXTL (*33*) as implemented on the Viglen Pentium computer. Crystallographic data and refinement details are presented in Table 1.

Table 1: Summary of Crystallographic Data for dppz·CH_3OH and [**1**][$(PF_6)_2$]·CH_3NO_2

	dppz[a]	[**1**][$(PF_6)_2$][b]
empirical formula	$C_{19}H_{14}N_4O$	$C_{21}H_{17}F_{12}N_5O_2P_2$
f_w	314.34	661.34
crystal system	monoclinic	triclinic
space group	$P2_{1/C}$ (C_2^5h, no. 14)	$P\bar{1}$ (C_1^1, no. 2)
crystal dimensions (mm)	0.50 × 0.12 × 0.12	0.45 × 0.43 × 0.10
a (Å)	4.5905 (12)	13.4948 (19)
b (Å)	12.887 (4)	13.8511 (19)
c (Å)	25.030 (7)	23.133 (3)
α (deg)		93.354 (3)
β (deg)	95.149 (6)	100.455 (3)
γ (deg)		119.018 (2)
U (Å^3)	1474.7 (7)	3664.0 (9)
Z	4	6
D_c (mg/m^3)	1.416	1.798
F(000)	656	1992
μ(Mo Kα) (mm^{-1})	0.092	0.303
final R1 (on *F*)[a]	0.0792	0.0919
final wR2 (on *F*)[a]	0.2402	0.2958

[a] A weighting scheme whereby $w = 1/[\sigma^2(F_o^2) + (0.1224P)^2 + 0.00P]$, where $P = (F_o^2 + 2F_c^2)/3$, was used in the latter stages of refinement. [b] A weighting scheme whereby $w = 1/[\sigma^2(F_o^2) + (0.1730P)^2 + 0.00P]$, where $P = (F_o^2 + 2F_c^2)/3$, was used in the latter stages of refinement.

UV−Visible Titrations. A stock 2.5 mM solution of the drug was made up in a 25 mM NaCl, 5 mM Tris, pH 7.0 buffer; 3000 μL of buffer was loaded into an optical glass cuvette with a path length of 1 cm, and 5 μL was removed with a Gilson pipette and replaced with 5 μL of the drug solution. This cuvette was then loaded into the spectrometer sample block, controlled at 25 °C; 3000 μL of the buffer was added to an identical cuvette and placed in the reference cell. Both the cuvettes were mixed 30 times with a Gilson 1000 μL pipette, and all bubbles were removed.

After the cuvettes had been allowed to reach equilibrium over the course of 30 min, a spectrum was recorded between 600 and 200 nm. Five to ten microliters of CT-DNA was added to both cuvettes and mixed 30 times. The spectrum was recorded after checking for bubbles and showed a drop in absorptivity showing interaction between the DNA and the drug. The titration was continued until there was no change in the spectrum indicating saturated binding

had occurred. Each titration was repeated at least three times.

Fluorescence Titrations. These titrations were carried out using a protocol similar to that used for the UV−visible titration, but since the fluorescence of the DNA and buffer is negligible, a reference cell was not used. Each titration was repeated at least three times.

Viscosity Measurements. Viscosity data were obtained using a Cannon-Fenske capillary viscometer submerged in a water bath at 27 °C. CT-DNA samples were first sonicated for 30 min. CT-DNA solutions were ~1 mM in base pairs, and flow times were recorded in triplicate using a digital stopwatch. All solutions were in a Tris buffer (5 mM Tris and 25 mM NaCl) at pH 7.

Isothermal Titration Calorimetry. ITC was carried out with approximately 290 μL of a 2.5 mM solution of [**1**][$(NO_3)_2$] loaded into the syringe, which was titrated into a 0.75 mM (base pairs) solution of CT-DNA at 25 °C in a 5 mM Tris, 25 mM NaCl, pH 7.0 buffer. After an initial injection of 3 μL, 18 injections of 15 μL each were performed with a separation of 300 s. The power required to return the system to thermal equilibrium was measured via the computer.

The experiment was repeated twice more, and heats of dilution experiments were also carried out, by diluting buffer into DNA, and DNA into buffer.

Computational Methods. All calculations were performed using Gaussian98 (*34*) using the B3LYP hybrid density functional method (*57*). The 6-31G* basis set was used for most calculations. The calculations were checked against more extended calculations using the 6-311+G(d,p) basis set. However, the results obtained in the larger basis set were not significantly different. Therefore, all results presented here were obtained using the smaller basis set. The coordinates for **1** were based on the crystal structure of [**1**][$(PF_6)_2$]. The molecular orbital plots were made using gOpenMol (*35*).

RESULTS

Structural Studies

Using a method adapted from the original synthesis by Dickson and Summers (*30*), [**1**][$(PF_6)_2$] was isolated in an improved yield (68% instead of 25% of the bromide salt) and fully characterized by ^{1}H NMR, FAB-MS, and elemental analysis. X-ray quality crystals of the hexafluorophosphate salt of **1** and dppz were obtained; somewhat surprisingly, the latter has not been reported previously. This allowed us to carry out a structural comparison of the two systems.

As might be expected, as an extended polyaromatic molecule, dppz is almost perfectly planar (Figure 1). The packing of the structure shows dppz molecules form offset stacks with face-to-face aromatic interactions reminiscent of graphite (Figure 1c). Such aromatic interactions have been observed in the crystal structures of other DNA intercalators (*28*, *36*), and the distance between ring planes is comparable to those seen in the base pair stacks of DNA (*37*).

The crystal structure of **1** shows that the accommodation of the ethylene group results in a slight twisting of the dppz moiety, although the structure is still very close to planarity (Figure 2). Packing is less ordered than in the dppz structure as the charge at the quaternized nitrogens, counterions, as well as solvent molecules must be accommodated. Nevertheless, there is evidence of stacking interactions between some of the rings of adjacent cations, with distances approaching 3.5 Å.

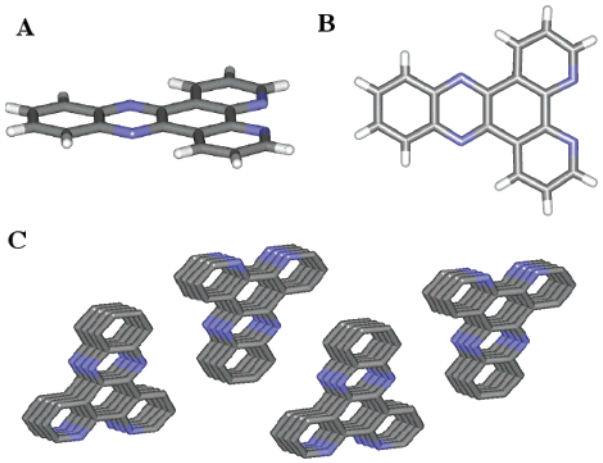

FIGURE 1: (a) Structural representation of the dppz molecule. (b) View of the same molecule after an ~90° rotation. (c) Crystal packing diagram of stacked dppz molecules. Hydrogen atoms and solvent molecules have been removed for clarity.

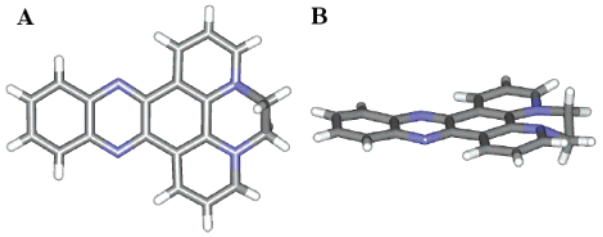

FIGURE 2: (a) Structural representation of the cation found in the crystal structure of [**1**][$(PF_6)_2$]. (b) View of the same cation after an ~90° rotation.

Photophysical Studies

Although the absorption spectrum of **1** has been previously reported (*30*), its luminescent properties have not been explored. Photoexcitation of acetonitrile solutions of [**1**]-[$(PF_6)_2$] at 325 or 415 nm results in unstructured luminescence which is slightly blue-shifted (λ_{em} = 515 nm) relative to that of the free base dppz, where structured emission is observed at 533 nm (λ_{em}) (*38*). Water-soluble [**1**][$(NO_3)_2$] was prepared by anion metathesis of the hexafluorophosphate salt with *n*-butylammonium nitrate. It was found that photoexcitation of aqueous solutions of [**1**][$(NO_3)_2$] resulted in unstructured emission centered at 510 nm (Figure 3).

Given that the cation of [**1**][$(NO_3)_2$] is luminescent, is almost as planar as the free base dppz, and also displays good water solubility, the interaction of **1** with DNA was investigated.

DNA Binding Studies

Binding Titrations. Initially, the interaction of [**1**][$(NO_3)_2$] with calf thymus DNA (CT-DNA) in aqueous buffer (25 mM NaCl, 5 mM Tris, pH 7.0) was investigated using absorption and emission spectroscopy.

Addition of CT-DNA to such solutions results in distinctive changes in the UV−visible spectrum of [**1**][$(NO_3)_2$], with the bands between 280 and 400 nm showing a high degree of hypochromicity. The higher-energy band also displays a

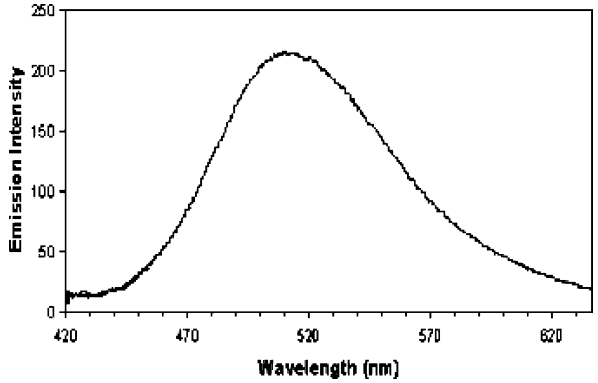

FIGURE 3: Emission spectrum of [**1**][$(NO_3)_2$] in water (λ_{ex} = 325 nm).

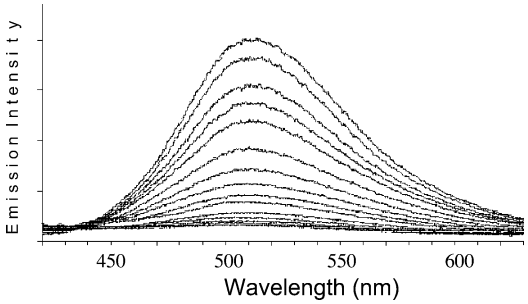

FIGURE 4: Emission quenching observed upon addition of CT-DNA to an aqueous buffer solution of [**1**][$(NO_3)_2$] (λ_{ex} = 415 nm).

Table 2: Summary of Binding Data for **1** with DNA, Determined by Spectroscopic Methods

	absorption titrations[a]		emission titrations[a]	
polynucleotide	S (bp)	K_b (mol^{-1} dm^3)	S (bp)	K_b (mol^{-1} dm^3)
CT-DNA	3.22	3.78×10^5	3.10	1.8×10^5
poly(dA)·poly(dT)	–	–	5.32	1.6×10^5
poly(dG)·poly(dC)	–	–	4.84	6.9×10^5

[a] Averaged values of several titrations. In each case, $R^2 > 0.95$. λ_{ex} = 415 nm.

bathochromic shift approaching binding saturation, while several isosbestic points are observed. These phenomena are characteristic of an interaction between the cation and the DNA helix, and the high percentage of hypochromicity is indicative of an intercalative interaction (*39*).

To avoid interference from the absorption bands of DNA, emission titrations were carried out at 415 nm (λ_{ex}). It was found that the emission spectrum of **1** was quenched by the addition of CT-DNA (Figure 4).

Luminescence Titrations with Other Polynucleotides. To further investigate the observed quenching effect, luminescence titrations of **1** with poly(dA)·poly(dT) and poly(dG)·poly(dC) were also carried out. In both cases, quenching analogous to that observed for CT-DNA was found to occur. The raw data obtained from the absorption and emission titrations were used to construct binding curves for the interaction of [**1**][$(NO_3)_2$] with CT-DNA, which were in turn fitted to the McGhee–von Hippel (MVH) model (*40*), resulting in the binding parameters shown in Table 2. Fits of these data to the MVH model offered some suggestion of a binding sequence preference for GC regions (Table 2). Additionally, it was noted that binding site sizes obtained in these experiments were consistently larger than those observed for CT-DNA. Attempts to reduce site sizes produced poorer data fits.

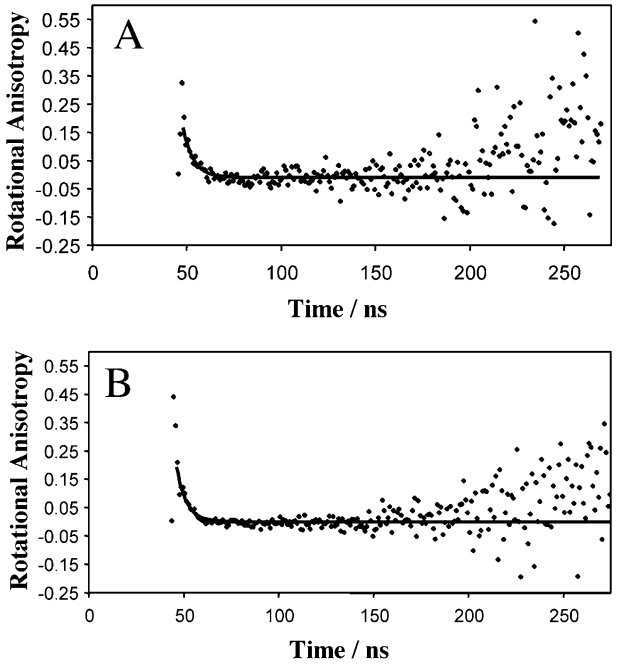

FIGURE 5: Decay of anisotropy with respect to time, for 2.5×10^4 M [**1**][$(NO_3)_2$] in 5 mM Tris (A) in the absence of CT-DNA or (B) with sufficient CT-DNA added to result in ~50% binding. Both curves were fitted using a single-exponential function [χ^2(A) = 1.210; χ^2(B) = 1.370].

Time-Resolved Anisotropy Measurements (TRAMS). TRAMS have previously been used to probe molecular dynamics (*41*), including DNA–intercalator interactions (*15*, *42*). To further investigate the reduction of the luminescent intensity for [**1**][$(NO_3)_2$] during DNA binding, time-resolved fluorescence anisotropy measurements on aqueous buffer solutions of **1** in the absence and presence of CT-DNA were taken. The raw data are shown in Figure 5.

A comparison of correlation lifetimes (τ_c) obtained from both experiments reveals that, within one standard deviation, they are identical (τ_c = 0.9 ns). The absence of a component with a longer correlation lifetime in the presence of DNA confirms that emission is exclusively from unbound **1** and that the bound cation is nonemissive. Furthermore, deconvolution of the time-resolved fluorescence intensity data reveals that the lifetime of the photoexcited state in water is 6.2 ns.

Viscosity Measurements. The observation of large hypochromicity and luminescent quenching is suggestive of an intercalative DNA binding mode for [**1**][$(NO_3)_2$]. However, a simple method for authoritatively distinguishing this binding mode involves viscosity experiments. Classical intercalation results in a lengthening of DNA, thus producing a concomitant increase in the relative specific viscosity of aqueous DNA solutions (*43*). Therefore, the effect of [**1**][$(NO_3)_2$] on the viscosity of aqueous CT-DNA solutions was investigated. It was found that the viscosity significantly increased upon addition of **1** (Figure 6). This observation is *a priori* evidence for an intercalative binding mode for **1**.

Calorimetry Studies

To obtain further insight into the thermodynamics of the DNA binding process, the interaction of [**1**][$(NO_3)_2$] with

Table 3: Summary of Thermodynamic Parameters Derived from ITC Studies for the Binding of **1** and Δ and Λ $[Ru(phen)_2(dppz)]^{2+}$ (data for metal complexes from ref *45*)

ligand	n	*S* (bp)	K_b (M^{-1} bp)	ΔH_B (kcal/M)	ΔG_{obs} (kcal/M)	$T\Delta S$ (kcal/M)
1	0.283	3.5	$(5.4 \pm 0.6) \times 10^4$	-2.6 ± 0.3^b	-7.4 ± 0.5^a	4.8 ± 0.6
Δ $[Ru(phen)_2(dppz)]^{2+}$		3.0	3.2×10^6	0.2	−8.9	9.1
Λ $[Ru(phen)_2(dppz)]^{2+}$		3.0	1.7×10^6	2.9	−8.5	11.4

[a] Values or ΔG_{obs} for all three compounds were determined using binding constants determined from either UV, fluorescence, or luminescence binding experiments. Thermodynamic data for Δ and Λ isomers of $[Ru(phen)_2(dppz)]^{2+}$ were determined in a 5 mM Tris, 50 mM NaCl, pH 7.0 buffer. [b] Enthalpy values were measured directly using isothermal titration calorimetry, and the standard relationship $\Delta G = \Delta H - T\Delta S$ was used to compute changes in entropy. Error values for the thermodynamic parameters associated with the binding of **1** are based on three separate ITC measurements.

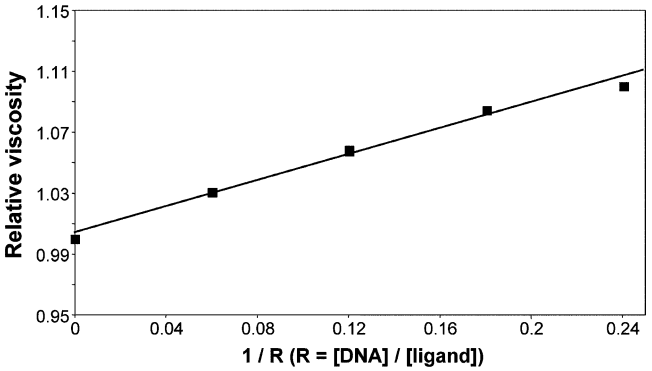

FIGURE 6: Plot of relative viscosity $(\eta/\eta_0)^{1/3}$ of CT-DNA vs $1/R$ for $[\mathbf{1}][(NO_3)_2]$ in a Tris buffer (5 mM Tris and 25 mM NaCl) at pH 7.

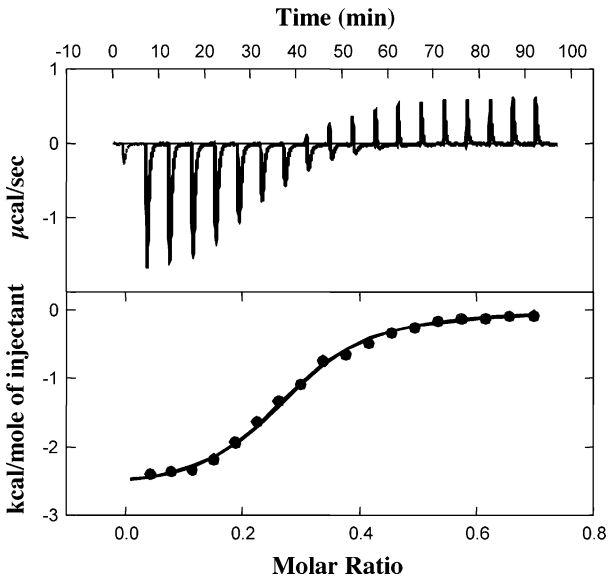

FIGURE 7: Raw ITC data for the titration of $[\mathbf{1}][(NO_3)_2]$ into CT-DNA at 25 °C.

CT-DNA was investigated using ITC (*31*, *32*, *44*). A typical titration is shown in Figure 7, while thermodynamic parameters are summarized in Table 3.

The top panel in Figure 7 shows the power compensation peaks produced after each serial injection of ligand into the sample cell containing DNA. Integration of these peaks with respect to time (and appropriate correction to a per mole basis) gives the corresponding binding isotherm in the bottom panel. The heats of ligand dilution were small and positive and did not vary as a function of ligand concentration, indicating that at the concentrations used in these experiments (typically, 2.0−2.5 mM) there is no significant ligand self-association. The heat of dilution was subtracted to give the corrected binding isotherm shown in the bottom panel of Figure 7. These data were best fit using a single set of identical binding sites model. It is self-evident that this model is not the correct one for this system given the nature of the DNA lattice used in these experiments, which has an array of potentially nonidentical intercalation sites. However, the sigmoidal nature of the binding curve gives no indication of more complex binding, and therefore, the use of more complex models to describe these data was not statistically justified.

The principal use of ITC in these experiments was to directly measure, and model independently, the binding enthalpy, which was found to be −2.6 kcal/mol. The equilibrium binding constant evaluated from spectroscopic titrations was used to determine the free energy change (ΔG_{obs}), and hence, the change in entropy could be calculated using standard relationships. These thermodynamic data are summarized in Table 3. For comparison, calorimetrically and spectroscopically determined thermodynamic data for the two isomers of $[Ru(phen)_2(dppz)]^{2+}$ are also included (*45*).

The overall thermodynamic picture that emerges from calorimetry experiments for the interaction of **1** with CT-DNA is that binding is both enthalpically and entropically favored. In addition, the binding of **1** is approximately 10-fold weaker than the interaction of the dppz complexed to the Ru^{II} center. The binding of the metal complexes is almost entirely entropic in nature with the enthalpy change in both cases being unfavorable. Clearly, the presence of a metal and coordinated phenanthroline rings has a major effect on the binding thermodynamics.

The site size, obtained from ITC for **1**, is in good agreement with values obtained from spectroscopic titrations and is entirely consistent with the neighbor exclusion model of intercalative binding. However, the value of K_b derived from the ITC experiments is 6 times lower than that obtained from spectroscopic titrations. The discrepancy between spectroscopically and calorimetrically determined binding constants is discussed further in the next section.

DISCUSSION AND THEORETICAL ASPECTS

Photophysical Properties of 1. The photophysical properties of **1** are striking. A comparison with $[Re(CO)_3(py)(dppz)]^+$ is particularly revealing. It has been established that luminescence of the metal complex is from a $^3\pi \rightarrow p^*$ state, and thus, as would be expected, the emission is structured with a long lifetime ($\tau > 100$ μs) (*18*−*20*). In contrast, the blue-shifted luminescence of **1** is unstructured with a short lifetime. Furthermore, a closer examination of the previously reported absorption spectrum for **1** in water reveals that, apart from the characteristic double-humped $\pi \rightarrow p^*$(dppz) transi-

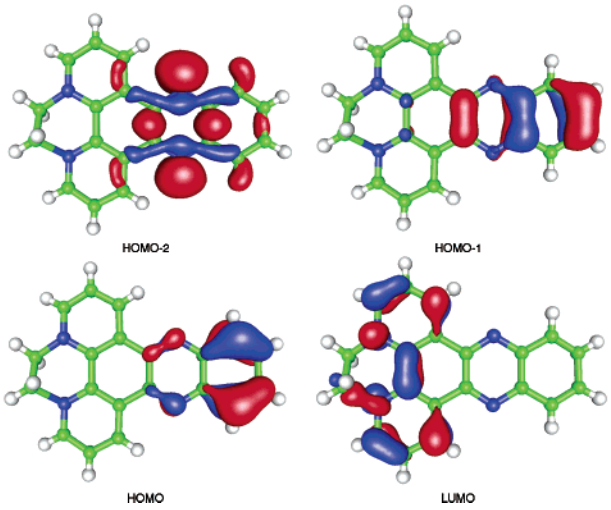

FIGURE 8: DFT-calculated frontier molecular orbitals for **1**.

tions at 364 and 380 nm, a relatively intense shoulder that extends past 410 nm is also observed. As discussed above, excitation into this band also results in emission at 510 nm. All these observations are indicative of intramolecular charge transfer (ICT). Thus, in comparison with other reported systems (*46*) containing analogous functional groups, the data are consistent with ICT from a HOMO centered on the electron-donating phenazine portion of **1** to a LUMO centered on the electron acceptor diquat moiety. Further support for this hypothesis is provided by density functional theory (DFT) calculations.

DFT Calculations. In contrast with dppz-based metal complexes, theoretical modeling of the entirely organic **1** is relatively facile. These calculations reveal that the three highest MOs of **1**, which are close in energy, are centered on the phenazine region of the molecule. In contrast, the LUMO of **1** is centered on the diquat region of the cation (Figure 8).

Further photophysical and theoretical studies will be required to ascertain the extent that solvent interactions modulate the ordering of the three occupied MOs from Figure 8, and to determine the precise character of the photoexcitation at 410 nm. However, it is clear that the calculations outlined above are consistent with photoexcitation into a ICT state.

Effect of DNA on Luminescence. DNA-induced luminescent quenching is a well-studied phenomenon (*47*, *48*). Indeed, several metal dppz-based complexes show emissions that are quenched upon interaction with polynucleotides (*49*). Even emissive states with lifetimes of nanoseconds can be quenched by this mechanism (*50*). Usually, this phenomenon is due to electron transfer from photo-oxidized guanine sites, but depending on excited state redox potentials, it can also involve adenine sites.

From polarography, the ground state one-electron reduction of [**1**][Br_2] in water occurs at an E_{red} of −0.40 V versus SCE (*21*), that is −0.16 V versus NHE. From these data, and the ΔE_{0-0} value of 2.43 eV, obtained from the emission maximum for **1**, the excited state reduction potential for **1** can be estimated from the relation $E_{red}^* = E_{red} + \Delta E_{0-0}$ (2.25 V vs NHE). From pulse radiolysis studies, the oxidation potentials of guanosine and adenosine are 1.58 and 2.03 V versus NHE, respectively (*51*). From these values, it is clear that the excited state of **1** is sufficiently reactive to photooxidize both guanine and adenine sites. More detailed studies on this process are underway.

Resolving the Discrepancy between Spectroscopic and Calorimetric Binding Constants. Examination of Tables 2 and 3 shows that binding constants determined from absorption and luminescence titrations differ from calorimetrically determined binding constants by ~5-fold at 25 °C, despite the use of identical buffer conditions. This discrepancy almost certainly arises from the fact that two different models have been used to fit the respective binding isotherms. In the case of the spectroscopic data, a neighbor exclusion model as described by McGhee and von Hippel was used. Calorimetric data were fit to a single set of identical binding sites model. In the neighbor exclusion model, the *K* parameter is the binding constant for the interaction of a ligand (drug) with an isolated binding site. In this context, "isolated site" refers to a stretch of DNA *n* base pairs long, where *n* is the exclusion parameter. For the ITC data, where a normal single set of sites model is used, the DNA concentration is set in base pairs and the molar binding ratio (*r*) is calculated, where $r = C_b/[S]_{tot}$ (C_b is the concentration of bound drug and $[S]_{tot}$ is the total concentration of binding site DNA in base pairs). Here the resultant *K* will *not* equal the *K* obtained from neighbor exclusion fitting. In fact, the two values should differ by the factor *n*, the exclusion parameter or the number of base pairs in the binding site. By making this correction, we find that within error the binding constants obtained from spectroscopy (2.8×10^5 M^{-1}) and calorimetry (1.9×10^5 M^{-1}) are in reasonable agreement.

*DNA Binding Thermodynamics of **1***. The affinity of compound **1** for CT-DNA is moderately high and in the normal range expected for simple intercalators. From Table 3, it is clear that the binding of **1** is 10-fold weaker than the binding of either Δ or Λ $[Ru(phen)_2(dppz)]^{2+}$. Isothermal titration calorimetry offers the most direct and model-independent method for measuring DNA binding enthalpies. In this study, we have for the first time measured the binding enthalpy of an "isolated" dppz moiety and found it to be small and negative. The negative sign for ΔH is typical for intercalation where stacking interactions with DNA base pairs stabilize the drug−DNA complex. For example, enthalpy values of −8.8 and −10.4 kcal/mol have been determined for ethidium and daunomycin, respectively (*52*, *53*). This is in contrast to the small positive enthalpy values measured for both the Δ and Λ isomers of $[Ru(phen)_2(dppz)]^{2+}$, despite the unambiguous demonstration of intercalation of these ligands (*11*−*20*, *45*). In the latter case, the overall thermodynamic profile was interpreted by suggesting that the favorable enthalpy that should arise from intercalative stacking is overcome by the energetic cost of placing bulky phenanthroline wings into the DNA grooves. At the same time, however, the positioning of the phenanthroline rings into the DNA grooves would give rise to a favorable entropy arising from the expulsion of site specifically bound water molecules. The overall observed thermodynamic parameters arise from a balance of opposing energetic factors.

The DNA binding thermodynamics of **1** are somewhat unusual since binding is both entropically and enthalpically favorable; however, the enthalpy is small in magnitude compared to the enthalpies of other simple intercalators. The positive $T\Delta S$ term is consistent with hydrophobic interac-

tions, where nonpolar groups are buried and made inaccessible to polar solvent. Intercalation of the dppz ligand is certainly consistent with this picture. If this were the case, then we would also expect a favorable (negative) enthalpy term to arise from van der Waals stacking interactions, and this is, in fact, exactly what is observed from the calorimetry data. Compound **1** is a dication at pH 7.0, and therefore, the interaction of this ligand with DNA is thermodynamically linked to the binding of sodium ions to DNA. This means that upon binding of **1** to DNA there is a stoichiometric release of condensed counterions from the DNA lattice. This polyelectrolyte effect is almost entirely entropic in nature, and therefore, this process must be a major contributor to the observed favorable entropy change that drives this interaction.

An additional source of favorable entropy consists of changes in the hydration state of both the ligand and the DNA. Disruption of bound water from the ligand or the DNA binding site would result in an unfavorable enthalpy but favorable entropy. This may be one of the reasons why the net enthalpy change is smaller in magnitude than what might be otherwise expected for intercalators of this type. We conclude therefore that the binding of **1** to DNA is primarily entropically driven. The molecular events that lead to this thermodynamic signature are likely to be counterion release upon binding of the dication, release of bound water from the ligand and/or the DNA binding site, and hydrophobic interactions arising from the removal of the ligand from aqueous bulk solvent into the interior of the DNA helix. A small negative enthalpy term, arising from stacking interactions with DNA base pairs, also makes a favorable contribution to the overall binding free energy.

For the Δ and Λ isomers of $[Ru(phen)_2(dppz)]^{2+}$, it is likely that unfavorable changes in configurational entropy arising from placing phenanthroline rings in the DNA grooves offset the favorable enthalpy that should be derived from stacking interactions. In addition, there is a small unfavorable enthalpy from removing hydration water molecules from the ligand upon binding. The net effect is a small unfavorable enthalpy. For compound **1**, however, there is no energetic cost of placing phenanthroline moieties into grooves, and therefore, in this case, the enthalpy is found to be negative. In both cases, binding is primarily entropic in nature, and possible sources for this are outlined above. However, the ruthenium compounds have a higher affinity, and this may result from additional and favorable hydrophobic interactions that come from placing the phenanthroline rings into the grooves (notwithstanding the unfavorable loss of configurational entropy) and the concomitant release of water and cations from the DNA grooves. Compound **1** does not pay as large an energetic "cost" as the Δ and Λ isomers of $[Ru(phen)_2(dppz)]^{2+}$ in DNA binding, but neither does it gain the large energetic "benefit" in binding that leads to the overall higher affinities of the metal complexes.

Location of Intercalation. It has previously been pointed out that the dppz ligand is structurally analogous to the naturally occurring antibiotic actinomycin d, a minor groove intercalator (*19*). Given this structural resemblance, the low steric demand of an essentially two-dimensional cation, the evidence of high solvent inaccessibility upon DNA binding, and the intercalative nature of this process, it seems highly likely that $[\mathbf{1}][(NO_3)_2]$ also binds from the narrow minor groove. Furthermore, the larger binding affinity of **1** for poly(dG)·poly(dC) is also consistent with this model as it is established that actinomycin d binds preferentially to specific GC sequences (*54*−*56*).

CONCLUSION

$[\mathbf{1}][(NO_3)_2]$ shows relatively good water solubility; this fact, and the distinctive photophysical properties of **1**, have allowed us to probe the nature of the interaction of a virtually isolated dppz unit with duplex DNA. The DNA binding affinity of **1**, while comparable to that of many metal complexes of dppz (*12*, *14*, *15*, *18*, *19*), is lower than that of the $[Ru(phen)_2(dppz)]^{2+}$ cation (*13*, *36*), and this can be explained by a consideration of the additional contribution of groove binding by the $[Ru(phen)_2)]^{2+}$ moiety for the metal complex.

More detailed biophysical and photophysical studies on the nature of the interaction of **1** with DNA, including an investigation of photoinduced redox processes, are ongoing. Synthetic studies on molecules related to **1**, designed to display targeted binding selectivities and higher affinities, are underway.

ACKNOWLEDGMENT

J.A.T. is grateful to Prof. A. Harriman for an illuminating discussion. We dedicate this paper to the memory of Professor Ian Soutar, whose untimely death has meant the loss of a valued friend and colleague.

SUPPORTING INFORMATION AVAILABLE

A diagram showing changes in the absorption spectrum of an aqueous buffer solution of $[\mathbf{1}][(NO_3)_2]$ upon progressive addition of CT-DNA and also luminescent quenching observed upon addition of poly(dA)·poly(dT) and poly(dG)·poly(dC) to an aqueous buffer solution of $[\mathbf{1}][(NO_3)_2]$. This material is available free of charge via the Internet at http://pubs.acs.org.

REFERENCES

1. Johnson, D. S., and Boger, D. L. (1996) DNA Binding Agents, in *Comprehensive Supramolecular Chemistry* (Atwood, J. L., Davies, J. E. D., MacNicol, D. D., and Vögtle, F., Eds.) Vol. 4, Pergamon, Oxford.
2. Zimmer, C., and Wahnert, U. (1986) Nonintercalating DNA-Binding Ligands: Specificity of the Interaction and Their Use as Tools in Biophysical, Biochemical and Biological Investigations of the Genetic Material, *Prog. Biophys. Mol. Biol. 47*, 31−112.
3. Thong, N. T., and Hélène, C. (1993) Recognition and Modification of Double Helical DNA by Oligonucleotides, *Angew. Chem., Int. Ed. Engl. 32*, 666−689.
4. Dervan, P. B., and Edelson, B. S. (2003) Recognition of the DNA minor groove by pyrrole-imidazole polyamides, *Curr. Opin. Struct. Biol. 13*, 284−299.
5. Wakelin, L. P. G. (1986) Polyfunctional DNA Intercalating Agents, *Med. Res. Rev. 6*, 275−340.
6. Geierstanger, B. H., and Wemmer, D. E. (1995) Complexes of the Minor Groove of DNA, *Annu. Rev. Biophys. Biomol. Struct. 24*, 463−493.
7. Faria, M., Wood, C. D., Perrouault, L., Nelson, J. S., Winter, A., White, M. R. H., Hélène, C., and Giovannangeli, C. (2000) Targeted Inhibition of Transcription Elongation in Cells Mediated by Triplex-forming Oligonucleotides, *Proc. Natl. Acad. Sci. U.S.A. 97*, 3862−3867.
8. Gottesfeld, J. M., Neely, L., Trauger, J. W., Baird, E. E., and Dervan, P. B. (1997) Regulation of Gene Expression by Small Molecules, *Nature 387*, 202−205.

9. Lippard, S. J. (1978) Platinum Complexes: Probes of Polnucleotide Structure and Antitumor Drugs, *Acc. Chem. Res. 11*, 211−217.
10. Sigman, D. S., Bruice, T. W., Mazumder, A., and Sutton, C. L. (1993) Targeted Chemical Nucleases, *Acc. Chem. Res. 26*, 98.
11. Nordén, B., Lincoln, P., Akerman, B., and Tuite, E. (1996) DNA Interactions with Substitution-Inert Transition Metal Ion Complexes, in *Metal Ions in Biological Systems* (Sigel, H., and Sigel, A., Eds.) Vol. 33, p 177, Marcel Dekker, New York.
12. Erkkila, K. E., Odum, D. T., and Barton, J. K. (1999) Recognition and Reaction of Metallointercalators with DNA, *Chem. Rev. 99*, 2777−2795.
13. Metcalfe, C., and Thomas, J. A. (2003) Kinetically inert transition metal complexes that reversibly bind to DNA, *Chem. Soc. Rev. 32*, 214−215.
14. Friedman, A. E., Chambron, J.-C., Sauvage, J.-P., Turro, N. J., and Barton, J. K. (1990) Molecular Light Switch for DNA: $Ru(bpy)_2(dppz)^{2+}$, *J. Am. Chem. Soc. 112*, 4960−4962.
15. Olson, E. J. C., Hu, D., Hörmann, A., Jonkman, A. M., Arkin, M. R., Stemp, E. D. A., Barton, J. K., and Barbara, B. F. (1997) First Observation of the Key Intermediate in the "Light-Switch" Mechanism of $[Ru(phen)_2dppz]^{2+}$, *J. Am. Chem. Soc. 119*, 11458.
16. Önfelt, B., Lincoln, P., Nordén, B., Baskin, J. S., and Zewail, A. H. (2000) Femtosecond linear dichroism of DNA-intercalating chromophores: Solvation and charge separation dynamics of $[Ru(phen)_2dppz]^{2+}$ systems, *Proc. Natl. Acad. Sci. U.S.A. 97*, 5708.
17. Jenkins, Y., Friedman, A. E., Turro, N. J., and Barton, J. K. (1992) Characterization of Dipyridophenazine Complexes of Ruthenium(II): The Light Switch Effect as a Function of Nucleic Acid Sequence and Conformation, *Biochemistry 31*, 10809−10816.
18. Lincoln, P., Broo, A., and Nordén, B. (1996) Diastereomeric DNA-Binding Geometries of Intercalated Ruthenium(II) Trischelates Probed by Linear Dichroism: $[Ru(phen)_2DPPZ]^{2+}$ and $[Ru(phen)_2BDPPZ]^{2+}$, *J. Am. Chem. Soc. 118*, 2644.
19. Tuite, E., Lincoln, P., and Nordén, B. (1997) Photophysical Evidence That Δ- and Λ-$[Ru(phen)_2(dppz)]^{2+}$ Intercalate DNA from the Minor Groove, *J. Am. Chem. Soc. 119*, 239−240.
20. Holmlin, R. E., Stemp, E. D. A., and Barton, J. K. (1998) $Ru(phen)_2dppz^{2+}$ Luminescence: Dependence on DNA Sequences and Groove-Binding Agents, *Inorg. Chem. 37*, 29−34.
21. Greguric, I., Aldrich-Wright, J. R., and Collins, J. G (1997) A ^{1}H NMR Study of the Binding of Δ-$[Ru(phen)_2DPQ]^{2+}$ to the Hexanucleotide $d(GTCGAC)_2$. Evidence for Intercalation from the Minor Groove, *J. Am. Chem. Soc. 119*, 3621−3622.
22. Hiort, C., Lincoln, P., and Nordén, B. J. (1993) DNA Binding of Δ- and Λ-$[Ru(phen)_2DPPZ]^{2+}$, *J. Am. Chem. Soc. 115*, 3448−3454.
23. Thorp, H. H. (1995) Electron-, Energy-, and Atom-Transfer reactions Between Metal Complexes and DNA, *Adv. Inorg. Chem. 43*, 127−177.
24. Che, C.-M., Yang, M., Wong, K. H., Chan, H.-L., and Lam, W. (1999) Platinum(II) Complexes of Dipyridophenazine as Metallointercalators for DNA and Potent Cytotoxic Agents against Carcinoma Cell Lines, *Chem.—Eur. J. 5*, 3350−3356.
25. Holmlin, R. E., Stemp, E. D. A., and Barton, J. K. (1996) $Os(phen)_2dppz^{2+}$ in Photoinduced DNA Mediated Electron-Transfer Reactions, *J. Am. Chem. Soc. 118*, 5236−5244.
26. Metcalfe, C., Adams, H., and Haq, I. (2003) A ruthenium dipyridophenazine complex that binds preferentially to GC sequences, *Chem. Commun.*, 1152−1153.
27. Soeffler, H. D., Thornton, N. B., Temkin, S. L., and Schanze, K. S. (1995) Unusual Photophysics of a Rhenium(I) Dipyridophenazine Complex in Homogeneous Solution and Bound to DNA, *J. Am. Chem. Soc. 117*, 7119−7128.
28. Yam, V. W. W., Lo, K. K. W., Cheung, K. K., and Kong, R. Y. C. (1995) Synthesis, Photophysical Properties and DNA-Binding Studies of Novel Luminescent Rhenium(I) Complexes: X-ray Crystal-Structure of $[Re(dppn)(CO)_3(Py)](Otf)$, *Chem. Commun.*, 1191−1193.
29. Dyer, J., Blau, W. J., Coates, C. G., Creely, C. M., Gavey, J. D., George, M. W., Grills, D. C., Hudson, S., Kelly, J. M., Matousek, P., McGarvey, J. J., McMasters, J., Parker, A. W., Towrie, M., and Weinstein, J. A. (2003) The photophysics of *fac*-$[Re(CO)_3(dppz)(py)]^+$ in CH_3CN: a comparative picosecond flash photolysis, transient infrared, transient resonance Raman and density functional theoretical study, *Photochem. Photobiol. Sci. 2*, 542−554.
30. Dickenson, J. E., and Summers, L. A. (1970) Dervatives of 1,10-Phenanthroline-5,6-quinone, *Aust. J. Chem. 23*, 1023.
31. Wiseman, T., Williston, S., Brandts, J. F., and Lin, L.-N. (1989) Rapid Measurement of Binding Constants and Heats of Binding Using a New Titration Calorimeter, *Anal. Biochem. 179*, 131−137.
32. Haq, I., Chowdhry, B. Z., and Jenkins, T. C. (2001) Calorimetric Techniques in the Study of High-Order DNA-Drug Interaction, *Methods Enzymol. 340*, 109−149.
33. *SHELXL, an integrated system for solving and refining crystal structures from diffraction data*, revision 5.1, Bruker AXS Ltd., Göttingen, Germany.
34. Frisch, M. J., Trucks, G. W., Schlegel, H. B., Scuseria, G. E., Robb, M. A., Cheeseman, J. R., Zakrzewski, V. G., Montgomery, J. A., Jr., Stratmann, R. E., Burant, J. C., Dapprich, S., Millam, J. M., Daniels, A. D., Kudin, K. N., Strain, M. C., Farkas, O., Tomasi, J., Barone, V., Cossi, M., Cammi, R., Mennucci, B., Pomelli, C., Adamo, C., Clifford, S., Ochterski, J., Petersson, G. A., Ayala, P. Y., Cui, Q., Morokuma, K., Rega, N., Salvador, P., Dannenberg, J. J., Malick, D. K., Rabuck, A. D., Raghavachari, K., Foresman, J. B., Cioslowski, J., Ortiz, J. V., Baboul, A. G., Stefanov, B. B., Liu, G., Liashenko, A., Piskorz, P., Komaromi, I., Gomperts, R., Martin, R. L., Fox, D. J., Keith, T., Al-Laham, M. A., Peng, C. Y., Nanayakkara, A., Challacombe, M., Gill, P. M. W., Johnson, B., Chen, W., Wong, M. W., Andres, J. L., Gonzalez, C., Head-Gordon, M., Replogle, E. S., and Pople, J. A. (2002) *Gaussian 98*, revision A.11.3, Gaussian, Inc., Pittsburgh, PA.
35. Bergman, D. L., Laaksonen, L., and Laaksonen, A (1992) A Graphics Program for the Analysis and Display of Molecular Dynamics Trajectories, *J. Mol. Graphics 10*, 33.
36. Gupta, N., Grover, N., Neyhart, G. A., Singh, P., and Thorp, H. H. (1992) $[RuO(dppz)(tpy)]^{2+}$: a DNA Cleavage Agent with High DNA Affinity, *Angew. Chem., Int. Ed. Engl. 31*, 1048−1050.
37. Voet, D., and Voet J. G. (1995) *Biochemistry*, 2nd ed., p 853, Wiley, New York.
38. Ackermann, M. N., and Interrante, L. V. (1984) Ruthenium(II) Complexes of Modified 1,10-Phenanthrolines. 1. Synthesis and Properties of Complexes Containing Dipyridophenazines and a Dicyanomethylene-Substituted 1,10-Phenanthroline, *Inorg. Chem. 23*, 3904−3911.
39. Holmlin, R. E., Yao, J., and Barton, J. K. (1999) Dipyridophenazine Complexes of Os(II) as Red-Emitting DNA Probes: Synthesis, Characterization, and Photophysical Properties, *Inorg. Chem. 38*, 174−189.
40. McGhee, J. D., and von Hippel, P. H. (1974) Theoretical Aspects of DNA-Protein Interactions: Cooperative and Noncooperative Binding of Large Ligands to a One-dimensional Homogeneous Lattice, *J. Mol. Biol. 86*, 469.
41. Soutar, I., Swanson, L., Christensen, R. L., Drake, R. C., and Phillips, D. (1996) Time-Resolved Luminescence Anisotropy Studies of the Relaxation Behavior of Polymers. 1. Poly(Methyl Methacrylate) and Poly(Methyl Acrylate) in Dilute Solutions in Dichloromethane, *Macromolecules 29*, 4931−4936.
42. Fiebig, T., Wan, C., Kelly, S. O., Barton, J. K., and Zewail, A. H. (1999) Femtosecond Dynamics of DNA-Mediated Electron Transfer, *Proc. Natl. Acad. Sci. U.S.A. 96*, 1187.
43. Satyanarayana, S., Dabrowiak, J. C., and Chaires, J. B. (1992) Neither Λ- nor L-tris(phenanthroline)ruthenium(II) Binds to DNA by Classical Intercalation, *Biochemistry 31*, 9319−9324.
44. Ladbury, J. E., and Chowdhry, B. Z. (1996) Sensing the heat: the application of isothermal titration calorimetry to thermodynamic studies of biomolecular interactions, *Chem. Biol. 3*, 791−801.
45. Haq, I., Lincoln, P., Suh, D., Nordén, B., Chowdrey, B. Z., and Chaires, J. B. (1995) Interaction of Δ- and Λ-$[Ru(phen)_2DPPZ]^{2+}$ with DNA: A Calorimetric and Equilibrium Binding Study, *J. Am. Chem. Soc. 117*, 4788−4796.
46. Metzger, M. (2003) Unimolecular Electrical Rectifiers, *Chem. Rev. 103*, 3803−3834.
47. Tuite, E. M., and Kelly, J. M. (1993) New trends in photobiology: Photochemical interactions of methylene blue and analogues with DNA and other biological substrates, *J. Photochem. Photobiol., B 21*, 103−124.
48. Seidel, C. A. M., Schulz, A., and Sauer, M. H. M. (1996) Nucleobase-Specific Quenching of Fluorescent Dyes. 1. Nucleobase One-Electron Redox Potentials and Their Correlation with Static and Dynamic Quenching Efficiencies, *J. Phys. Chem. 100*, 5541−5553.

49. Moucheron, C., Kirsch-De Mesmaeker, A., and Kelly, J. M. (1997) Photoreactions of Ru(II) and Os(II) complexes with DNA, *J. Photochem. Photobiol., B 40*, 91−106.
50. Reid, G. D., Whittaker, D. J., Day, M. A., Turton, D. A., Kayser, V., Kelly, J. M., and Beddard, G. S. (2002) Femtosecond Electron-Transfer Reactions in Mono- and Polynucleotides and in DNA, *J. Am. Chem. Soc. 124*, 5518−5527.
51. Steenken, S., and Jovanovic, S. V. (1997) How Easily Oxidizable Is DNA? One-Electron Reduction Potentials of Adenosine and Guanosine Radicals in Aqueous Solution, *J. Am. Chem. Soc. 119*, 617−618.
52. Hopkins, H. P., Fumero, J., and Wilson, W. D. (1990) Temperature-Dependence of Enthalpy Changes for Ethidium and Propidium Binding to DNA: Effects of Alkylamine Chains, *Biopolymers 29*, 449−459.
53. Chaires, J. B., Priebe, W., Graves, D. E., and Burke, T. G. (1993) Dissection of the Free-Energy of Anthracycline Antibiotic Binding to DNA: Electrostatic Contributions, *J. Am. Chem. Soc. 115*, 5360−5364.
54. Jain, S. C., and Sobell, H. M. (1972) Stereochemistry of Actinomycin binding to DNA II. Detailed Molecular Model of Actiomycin-DNA Complex and its Implications, *J. Mol. Biol. 68*, 21−34.
55. Fox, K. R., and Waring, M. J. (1984) DNA Structural Variations Produced by Actinomycin and Distamycin as Revealed by DNAase-I Footprinting, *Nucleic Acids Res. 12*, 9271−9285.
56. Kamitori, S., and Takusagawa, F. (1992) Crystal Structure of the 2/1 Complex Between D(GAAGCTTC) and the Anticancer Drug Actinomycin-D, *J. Mol. Biol. 225*, 445.
57. Becke, A. D. (1993) Density functional thermochemistry. III. The role of exact exchange, *J. Chem. Phys. 98*, 5648−5652.

BI049146R